DESIGN AND TEST OF A UAV BLENDED WING BODY CONFIGURATION

Kai Lehmkuehler*, KC Wong* and Dries Verstraete*
***School of Aerospace, Mechanical and Mechatronic Engineering, The University of Sydney, Australia**
kai.lehmkuehler@sydney.edu.au

Keywords: *Blended Wing Body, UAV, Wind tunnel, Stability, Propulsion Effects*

Abstract

This paper presents the design and test of a UAV blended wing body configuration. It is the result of a global student design project between the University of Sydney, the University of Colorado and the University of Stuttgart. Firstly, the design methodology and constraints are introduced. Then the wind tunnel test setup is described and the data presented. Finally, an engineering method to predict the propulsion effects on this unusual airframe is described.

Comparison between the wind tunnel data and panel code predictions shows good agreement, also reinforced by successful flight tests.

Propulsion effects on a low stability airframe can be serious and need to be considered during the design to avoid possible instabilities. The method presented allows for a quick estimate without tedious computations or tests.

1 Introduction

Blended wing body (BWB) configurations have attracted considerable interest lately as an alternative, more efficient platform for transport aircraft [1][2]. In conventional tube-wing configurations the fuselage typically contributes only minor amounts of lift while adding considerable skin friction drag as well as a disruption of the lift distribution across the wing. BWBs locate their payload volume inside the wing such that the entire external surface contributes to the generation of lift and the aircraft can be shaped for an optimal lift distribution. Typically they also are tailless flying wings which potentially further reduces the drag.

The use of BWBs for full scale transport aircraft is still some time away due to several problems; mainly the compliance with current regulations is difficult if not impossible (passenger evacuation, aircraft control without artificial stability and so on). Another application for a BWB might be a smaller, unmanned platform, where most of these constraints do not apply but high efficiency and large internal volume are required. Therefore the aim of this project is to design and test a small scale BWB and to determine if the platform is a viable configuration as a UAV.

The aircraft discussed in this paper is the first iteration of the project. It was designed for the international Hyperion project, which was a cooperation of student teams from Sydney, Australia, Stuttgart, Germany and Colorado, USA. The Sydney team was tasked with the airframe conceptual design and the wind tunnel testing. The plane was built in Germany and the US, where it was flown successfully in April 2011.

This paper will outline the design and testing conducted before the first flight. Future publications will cover the flight testing and the continuing development of the platform.

2 Design Methodology

There was a constraint of 9 calender months to take the project from requirement definition to first flight. Thus time was limited for the conceptual design phase. Subsequently, the focus was put on stability and control of the aircraft, with an optimisation for minimum drag to follow in a later stage.

A tailless aircraft has some unique requirements for stable flight especially in the pitch axis. The moment arm between the CG and the elevator is short and the design is a compromise between the static margin and the elevator effectiveness. The two extremes are:

1. A forward neutral point (NP) gives good elevator effectiveness but it will be difficult to place the CG sufficiently forward of the NP to ensure pitch stability.

2. An aft NP allows for a more practical CG placement but the elevator moment arm becomes shorter which makes trim difficult with sensible elevator sizes. In this arrangement it is also difficult to achieve appropriate pitch damping.

The preliminary design was done in AVL [3], which allows for quick evaluations of different airframe shapes with immediate output of all stability derivatives. The design was later investigated with PanAir [4], a fully 3-d panel code, and the results compared to AVL and the wind tunnel data.

The basic parameters for the aircraft were: 16kg MTOW, 3m span and 15m/s stall speed. Together with the general requirements of a flying wing mentioned above, this placed some very difficult constraints on the design, especially for the test flights in Colorado which is at an altitude of 1600m above sea level. A BWB cannot have flaps due to the additional pitching moment. Hence the clean airframe had to produce a maximum lift coefficient of at least 0.8, which is more than has been reported by other designs of this type [5]. The constraint on the wing span limited the aspect ratio and therefore the maximum wing area possible.

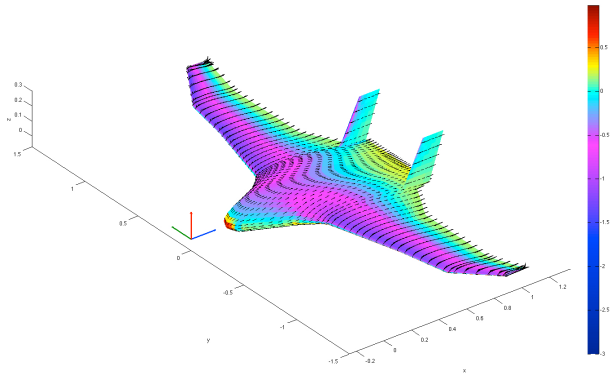

Fig. 1 PanAir model with pressure distribution and surface flow directions

All BWBs currently under investigation in literature have highly swept wings for their transonic flight regime. As this aircraft is flying subsonic at all times the wing sweep was limited to 15 degrees (for roll stability) to avoid tip stall tendencies associated with higher sweep at high lift coefficients.

As for any flying wing, the aerofoils used require a very low moment coefficient, which typically leads to reflexed sections. For a small UAV the low flight speed and wing chord also requires good performance at low Reynolds numbers. The aerofoils for the plane were selected based on the excellent website for model aircraft builders [6], which provides comprehensive information on low Reynolds number, low pitching moment aerofoils. The chosen section was the S5010 [7] aerofoil, which is 10% thick. For the body section, the aerofoil was modified in X-Foil [8] into a S5016 with 16% thickness to provide the required volume.

The design process for the shape of the aircraft was basically a manual exploration of the design space with several configurations and trends examined by hand until an arrangement was found to fit the requirements. A formal optimisation process was not possible due to the time constraints. Further work since then has determined that within the requirements and constraints there is no significant improvement possible unless the wingspan constraint was relaxed.

The final airframe shown in Figures 1 and 12 features a tractor propeller in the nose, which was chosen over an initial pusher concept mainly because of clearance issues during rotation and weight and balance advantages. The propeller is also more efficient when not running in the flow field of the main body. Other configuration decisions include:

- A single large elevator 20% of the main body chord to ensure enough control power for all flight phases;
- Twin fins on each side of the elevator the size of which was determined from the suggested values for the weathercock stability $C_{n\beta}$ in [9];
- Upwards canted swept back wing tips for additional dihedral;
- Tricycle landing gear; and
- The final wing area being 1.53 sqm with a body length of 1.25m.

3 Wind Tunnel Set-up

The department's 7x5 feet low speed wind tunnel was the ideal venue for testing this airframe, as it could accommodate a half-scale model at the required speed range to match the Reynolds numbers between the test and the flight airframe.

To perform the tests for this aircraft, the full flight envelope in angle of attack and sideslip was required. The existing balance could move only in angle of attack with the model suspended from the roof. It was thus required to design a new balance using the existing turntable mechanism. The design chosen was a single sting balance with an internal loadcell as shown in Figure 2. The model is driven by an actuator in angle of attack on top of the sting and the entire mechanism rotates in sideslip on the turntable. The loadcell processing and the motion control is handled in a newly developed graphical MatLab application, which allows control of all features from a single GUI. An image of the setup is shown in Figure 3.

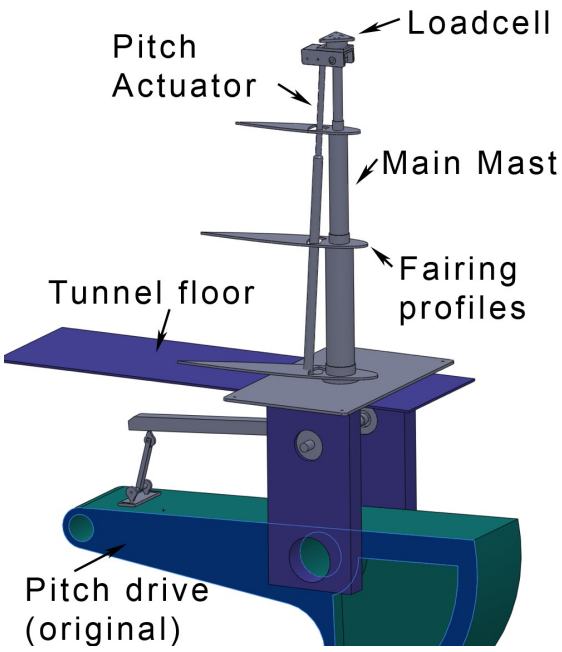

Fig. 2 CAD model of the new 6 axis wind tunnel balance

The model was constructed using the recent in-house completed CNC hot wire cutter, which was built by the UAV design group. The machine allows to cut linearly tapered foam blocks with good precision but it cannot generate the curvatures required for the blended shape. These were finished by hand after the assembly of the blocks into the complete airframe. This method of construction allows for a reasonably quick model construction on a limited budget but the final result has inevitably some tolerances due to the small scale and manual re-work. This was to show up later in the wind tunnel results but were considered acceptable for this first demonstrator airframe. A second limitation for the testing is the lack of stiffness of the available load cell in the roll axis. Hence the model vibrates slightly in roll, especially near stall, where the vortex shedding from the wing tips becomes more severe. As expected, the roll moment data shows more error than the other axes but the data was still usable as discussed below.

The model features an interchangeable nose section for powered testing and removable wing tips to evaluate different designs.

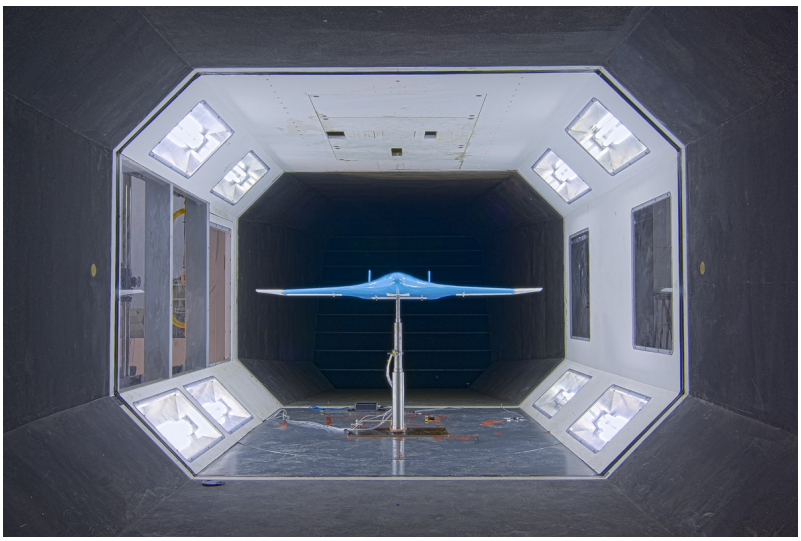

Fig. 3 Wind tunnel installation with fairings removed

4 Test Results for the Unpowered Airframe

This section presents the test results for the half-scale airframe model using the new balance. The data represents the current status of maturing experimental setup. Thus some minor errors are expected to be in the data. The data has been corrected for the changing gravity vector during angle of attack changes but no corrections have been applied for wind tunnel effects like blockage. Those are still under investigation.

All data is reported at 20m/s tunnel speed, which represents a Reynolds number of 450,000 based on the mean aerodynamic chord. Where applicable, changes due to different airspeeds are discussed. On all plots blue dots represents the experimental data points, solid red the appropriate fit and dashed black the data from PanAir. As a comparison, data from AVL has been included, too to judge the performance of this code against PanAir for an unusual airframe concept.

4.1 Lift

The lift curve shown in Figure 4 matches the predictions closely. The error is less than 2% at 20m/s. At lower speeds the difference reduces (no error at 13m/s) and it increases with airspeed. The aircraft has a relatively low aspect ratio of 5.9, so the slope of the lift curve is low as expected.

$C_{L\alpha}$ experiment	4.15 / rad
$C_{L\alpha}$ PanAir	4.23 / rad
$C_{L\alpha}$ AVL	4.016 / rad
$C_{L,max}$ experiment	0.946

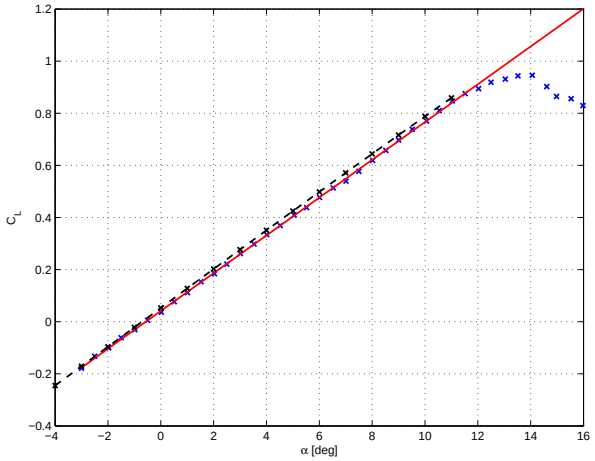

Fig. 4 Lift coefficient at 20 m/s

The maximum lift coefficient increases with airspeed to 0.96 from 0.93 at 13m/s. This is caused by the increase in Reynolds number over the wings.

The stall pattern is well behaved with flow separation starting at the inboard wing joint as predicted. The wing tips with the sharp break in the leading edge stall at about the same time but the flow separation does not spread inboard. The shape of the wing tips is currently under revision for that reason.

4.2 Drag

The drag polar in Figure 5 shows a small shift between the experiment and the predictions. The wind tunnel data has the minimum drag at $C_L \approx 0.1$ compared to $C_L \approx 0.05$ from PanAir. This can be caused by small differences in the geometry of the model to the PanAir geometry.

The span efficiency is generally lower than the inviscid predictions up until 30m/s, where it then matches. This is caused by the low Reynolds numbers, which are not taken into account by the panel methods. The AVL prediction for the span efficiency is very optimistic, with the difference caused mainly by small differences compared to PanAir around the zero-lift drag. This leads to large changes in the quadratic fit used to find e.

Span efficiency e experiment	0.72
Span efficiency e PanAir	0.77
Span efficiency e AVL	0.98
$C_{D,0}$ experiment	0.015

As mentioned before, this aircraft was mainly designed for stability and control properties with only limited effort on optimising the flight performance. The high induced drag has since then been investigated and identified to be caused by the sudden, large change in chord in the body-wing transition and the low aspect ratio. These findings will be used for the next iteration of the vehicle design.

A model aeroplane style fixed landing gear has also been tested in the wind tunnel. On this scale a landing gear is usually large compared to the rest of the airframe dimensions to deal with rough landing strips used to fly these planes. Here the landing gear adds about 30% to the zero lift drag. Clearly, this eliminates any performance gain of the blended airframe and should be avoided.

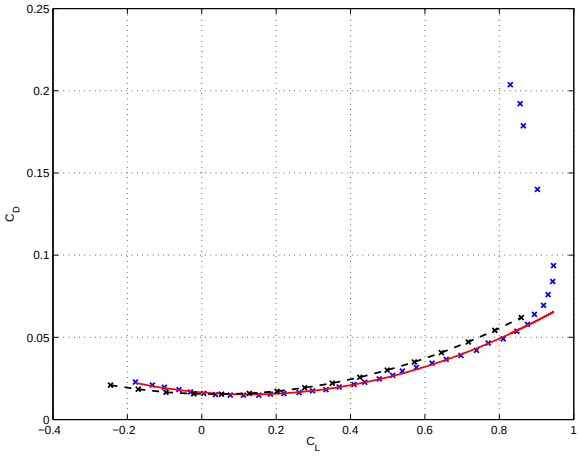

Fig. 5 Drag polar at 20 m/s

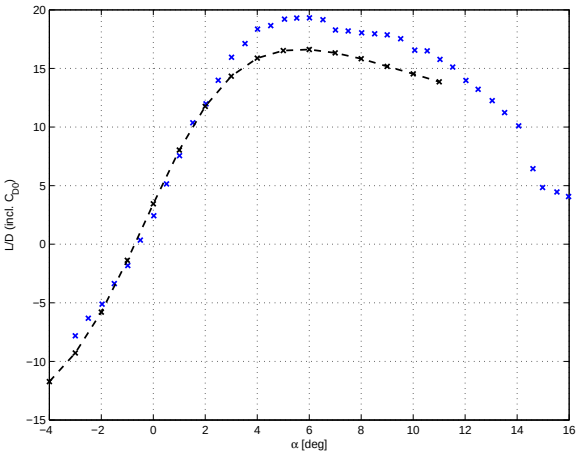

Fig. 6 L/D at 20 m/s

The combination of low aspect ratio and high induced drag results in a maximum L/D of 19.3 as shown in Figure 6. While this should improve in future versions of the airframe, it is still a respectable value for a low aspect ratio aeroplane at low Reynolds numbers.

4.3 Pitching Moment

There is a 8% error in the pitching moment slope as shown in Figure 7. This is mainly caused by the limited accuracy of the model (especially the reflexed aerofoils on the wings) and also some uncertainty in the location of the mounting point

for the loadcell. A change in CG position of only 3mm eliminates the error completely.

The CG range of the aircraft is very small, with only 30mm between instability and the limits of the elevator effectiveness. The flight CG has been placed at $x = 0.6m$ based on pilot comments.

The landing gear tests revealed only negligible increases in nose down pitching moment due to the additional drag of the gear.

$C_{m\alpha}$ experiment	-0.57 / rad
$C_{m\alpha}$ PanAir	-0.62 / rad
$C_{m\alpha}$ AVL	-0.564 / rad
NP experiment	0.646 m

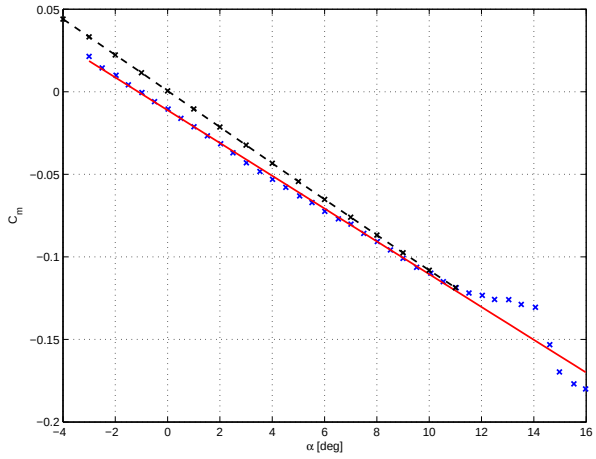

Fig. 7 Pitching moment at 20m/s with $X_{ref} = 0.55m$

4.4 Side force

The side force derivative shows good agreement between predictions and the experiment.

$C_{y\beta}$ experiment	-0.1863 / rad
$C_{y\beta}$ PanAir	-0.1835 / rad
$C_{y\beta}$ AVL	-0.187 / rad

4.5 Rolling moment

The experimental data for the rolling moment in Figure 8 shows more fluctuations than the other axes. This is due to the vibrations of the model about the roll axis on the loadcell as discussed before.

The value of the derivative matches the AVL prediction quite well but there is a large error to the PanAir computation. The reason for this error has not yet been determined.

$C_{l\beta}$ experiment	-0.059 / rad
$C_{l\beta}$ PanAir	-0.0258 / rad
$C_{l\beta}$ AVL	-0.059 / rad

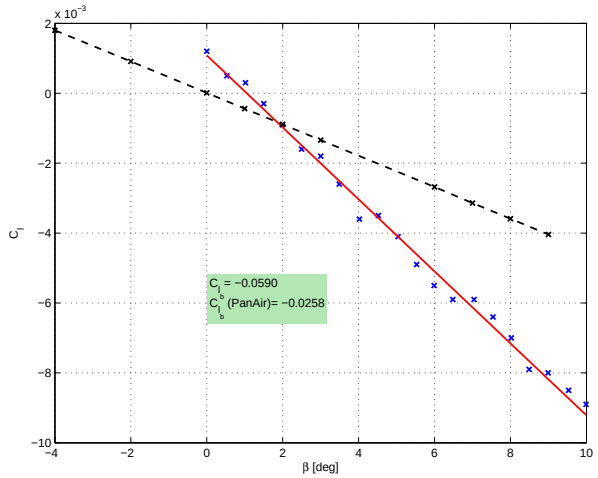

Fig. 8 Rolling moment at 20m/s

The airframe has no dihedral for ease of construction and was designed to obtain its roll stability from the limited wing sweep and the body-wing flow field. The upward canted wing tips provide further stability but this is not really required, based on the first flight tests.

4.6 Yawing moment

The yawing moment shown in Figure 9 is slightly stiffer than predicted but the derivative is still below the recommended value of $C_{n\beta} = 0.05$ [9]. This can be easily fixed by slightly larger fins but again has been found to be not necessary during the initial flight tests.

$C_{n\beta}$ experiment	0.0365 / rad
$C_{n\beta}$ PanAir	0.033 / rad
$C_{n\beta}$ AVL	0.03445 / rad

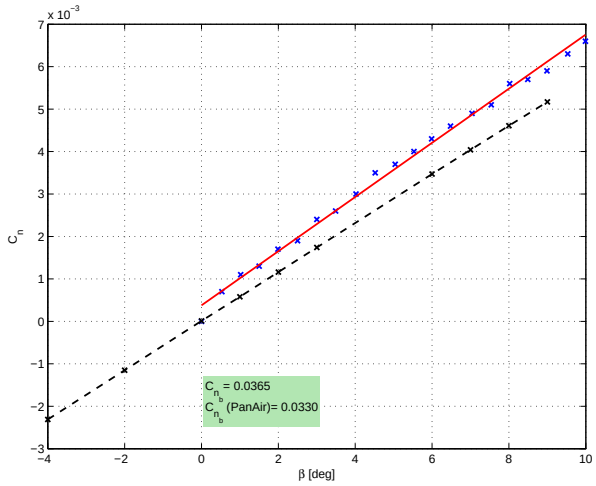

Fig. 9 Yawing moment at 20m/s

Fig. 10 First flight of the full scale Hyperion BWB in Boulder, Colorado

4.7 Pilot feedback

The airframe has been flown by several pilots, full (Figure 10) and half-scale versions in the U.S.A. and a half-scale version in Australia. Pilots' feedback on the handling qualities reported good characteristics in flight and some difficulties on take-off and landing. In flight, the aircraft was reported quite stable in all three axes with some minor adverse yaw. It was well controllable in all manoeuvres tested with well damped modes of motion. The amount of elevator to trim is relatively large but this is expected for a flying wing configuration.

On take-off, a reduced longitudinal stability was observed due to propulsion effects as discussed below. This was manageable in the U.S.A. as the flights there were done on a sealed runway and therefore very limited disturbances during the critical speed range. In Australia, there is no convenient access to such a runway, so grass fields were used. Here the natural unevenness of the ground has caused more severe issues during the take-off run with several premature lift-offs below rotation speed.

On landing, the reduced pitch damping makes it difficult to flare due to phugoid oscillations. This issue can be improved with better pilot training but it is intended that subsequent designs will improve on these undesired handling qualities.

5 Propulsion Effects

Any airframe shows some effect of its propulsion system on its stability characteristics [10]. For example, on a conventional, propeller-driven general aviation aircraft, the swirl of the prop wash impacting the vertical stabilizer causes a yawing moment. Likewise, on a jet with underwing engines there is a thrust dependent pitch up effect.

This BWB configuration with a tractor propeller in the nose shows an additional behaviour. The propeller is effectively blowing the inboard sections of the body behind it, causing a locally different dynamic pressure over these aerofoils. This thrust and airspeed dependent effect changes the moment balance between the the body and the outer wings. As the body creates more lift in the slipstream compared to the non-powered airframe, its more forward neutral point becomes more dominant and the overall NP moves forward. With the limited CG range of the configuration, this may have a severe effect, as the NP could potentially move in front of the CG during low airspeed, full power flight conditions, causing pitch instability.

With the limited time frame of the project spent predominantly with the basic design and

testing, this effect was not investigated until shortly before the first flight. After it became apparent that this might have catastrophic effects during the take-off run, a quick method to estimate the magnitude of the NP movement was required. Further wind tunnel work was impossible at that stage and there is no quick way of simulating these non-uniform inflows in the analysis tool used for this project. Thus a method was devised using the PanAir results, which is presented below.

PanAir reports all forces and moments for the entire airframe and also for each parallel, spanwise panel strip (Figure 12) from the leading edge to the trailing edge. Instead of calculating the NP from the full aircraft data with

$$\bar{X}_{NP} = \bar{X}_{CG} - \frac{C_{m\alpha}}{C_{L\alpha}} \tag{1}$$

it is possible to calculate the NP of every strip and find the overall NP by a weighted average of all strips. Then, using the velocity profile behind a propeller from a blade element code, each strip can be adjusted to the local dynamic pressure to simulate the effect of the prop-wash. The steps in detail:

1. Determine the slipstream velocity distribution for the propeller with a blade element code. The propeller for the aircraft had 4-blades and 20 inch diameter. As the aerofoils on the model aircraft propellers are usually not known, a simple Clark Y section was run in X-foil at the 75% station at full power. Here the propeller speed was 8000 RPM, giving a Reynolds number of 230000 at Mach 0.5. The lift curve and drag polar at that flow condition were determined and used in the blade element code. Tip losses were added by imposing zero velocity at the propeller tips. The propeller had 10 inch geometric twist along the blade.

2. Using this data shown in Figure 11, the local dynamic pressure seen by every strip can be interpolated.

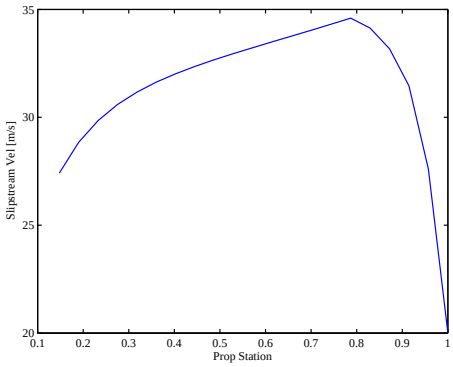

Fig. 11 Slipstream velocities for full power at $V_\infty = 20$m/s

3. Dimensionalise the lift and pitching moment of every strip using the local dynamic pressure to obtain the actual forces and moments acting on each strip.

4. Determine the NP of every strip using eq. 1. This requires a PanAir solution at two angles of attack to determine the lift- and moment curve slopes.

5. Calculate the NP of the aircraft by applying a weighted average for each strip based on the amount of lift produced compared to the total lift.

6. Compare the result to the NP of the unpowered aircraft for several airspeeds.

After adjusting the NP of the PanAir results to match the wind tunnel results by a small reference point change as mentioned above, a test case with zero slipstream yields $X_{np} = 0.645m$ vs. $X_{np} = 0.644m$ for the full aircraft calculation. This small difference is probably caused by internal round off errors as the coefficients are only available to 5 digits in the PanAir solution file. A further source of error might be the weighted averaging based on the lift produced per strip. However, the difference is small for practical use, so no further improvements were attempted.

Crucial for the method to predict useful results is the number of panel strips affected by the

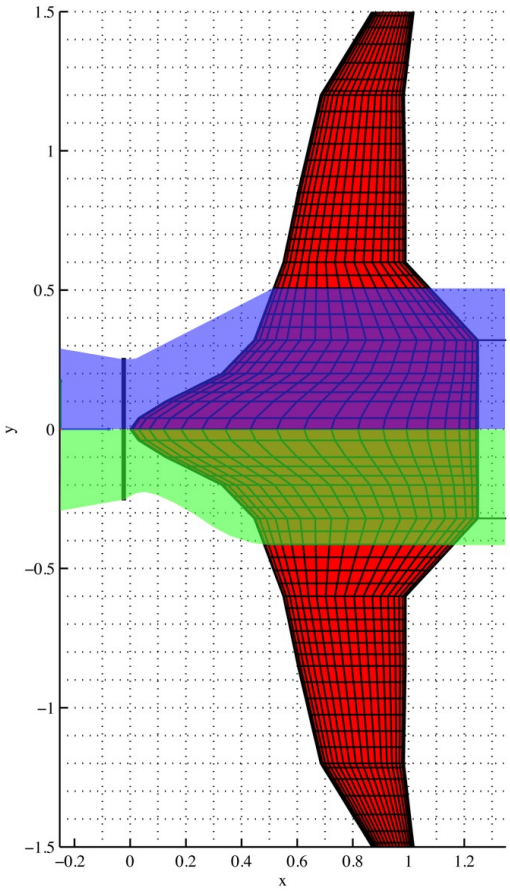

Fig. 12 Propeller slipstream distribution (Assumption blue (top), Experiment green (bottom)

slipstream. Several graphs of propeller body interference are given in [11]. There it can be seen that the typical contraction of the slipstream behind the propeller disc does not happen due to the presence of the body blockage. Instead, the slipstream follows the contour of the body. To estimate the affected area of the BWB this data was combined with some flow visualisation done on the un-powered model in the wind tunnel before. It was assumed that the slipstream follows the contour of the body up to the impact with the wing as shown in the top half of Figure 12 in blue. Over the wing it would then align with the free stream. This distribution results in 12 strips, or 1.9 times the prop diameter, being affected by the slipstream and hence the blade element results were interpolated over these 12 strips as shown in Figure 12.

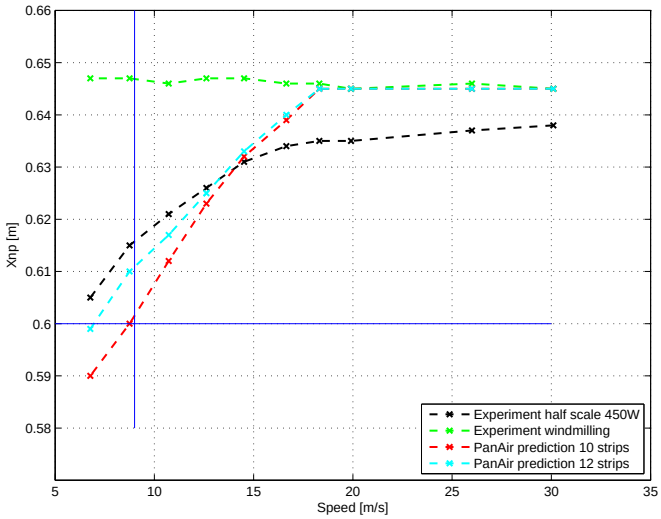

Fig. 13 NP changes due to propulsion effects (Indicated are the stall speed and flight CG)

The result of these computations show a NP shift forward during slow, high power conditions from $X_{np} = 0.645m$ to $X_{np} = 0.61m$ at stall speed. That means that the static margin just before rotation is reduced to 1.4%, down from 6.4% at cruise. This is clearly a severe effect and was observed during the take off runs preceding first flight with the aircraft pitching up uncontrollably during acceleration. Subsequently, based on this analysis, the CG was placed further forward and the flight was a success.

6 Test Results for the Powered Airframe

To verify the results, powered tests were performed using the half- scale wind tunnel model. It was powered by a 550W motor driving a 10 inch propeller with two blades. To achieve reasonably similar conditions, the test airspeeds were scaled by $l^{0.5}$ and the power was scaled as $l^{3.5}$, from 5000W on the full scale aircraft to 450W. The data is plotted in Figure 13, scaled to the experiment speeds. To start with, it was investigated if the unpowered, windmilling propeller had any influence on the NP (green). It can be seen that at low speed the effect is negligible, but at higher airspeeds there is a small shift forward.

The results of the powered experiment are plotted in black. They match the computations (cyan) well around the stall speed (14% difference in NP shift) but diverge at high speeds. Here the real propeller is still generating thrust while the blade element code shows windmilling from 18m/s. This is caused by inaccuracies in the propulsion model, which amongst others ignores the effects of the body blockage and changes to the flow direction through the propeller disc. Improvements on the modelling of these effects should increase the accuracy of the simulation, but this was impractical for the simplistic approach taken.

The assumed flow field over the aircraft was investigated on the model with tufts and a rake tracing the propeller tip vortex. The result is shown in Figure 14 with the blue string and has been indicated on Figure 12 in the lower half. The stream tube right behind the prop contracts the usual way contrary to the assumption. The highly tapered body does not produce enough blockage to match the results from [11], which used a blunter body. Further down the the flow aligns with the body contour as expected and then it curves in over the wing leading edge. From 10% chord the slipstream is aligned with the free stream to the trailing edge. The measured distance from the centreline is 190mm, which translates into 10 strips or 1.5 times the propeller diameter on the PanAir model in Figure 12. Therefore, the affected portion of the airframe was slightly overestimated. A calculation with 10 strips is shown in red in Figure 13. The NP shift becomes more severe at low speeds as the slipstream is concentrated over the inboard parts of the BWB. This means that the propulsion model produces too much thrust at these low speeds, which will be caused by the simplifications mentioned above. Again, a better model should improve the accuracy.

The presented method shows a simplified, but fast way of determining the propulsion effect on this BWB airframe. It was very helpful understanding the effect and it is conservative as it over-predicts the effect by a reasonable amount. The results of the method were crucial for the success of the first flight and will be tested on future versions of the aircraft with different body shapes to explore its versatility.

Fig. 14 Prop wash boundary as determined in the wind tunnel for a 10 inch propeller

7 Conclusion and Future Work

This paper presented a design and testing of a blended wing body UAV airframe. The design methodology using fast panel methods has been proven viable for an unusual configuration. The wind tunnel tests matched the predicted data well and the flight testing revealed good handling qualities in flight. Some problems during take off and landing due to the limited aircraft stability and the presence of propulsion effects on the longitudinal stability remain. The method used to obtain an engineering estimate of these effects has been proven usable.

Future development of the airframe will focus on improving the induced drag properties and the remaining stability issues. A full flight instrumentation system is currently being developed to perform flight testing for parameter estimation purposes.

References

[1] Hileman, J. I., Z. S. Spakovszky, et al. (2007). "Airframe Design for Silent Aircraft." 45th AIAA Aerospace Sciences Meeting and Exhibit 8 - 11 January 2007, Reno, Nevada.

[2] Liebeck, R. H. (2004). "Design of the Blended Wing Body Subsonic Transport." Journal of Aircraft 41(1).

[3] Drela M. (2011). AVL. Retrieved 15.3., 2012, from web.mit.edu/drela/Public/web/avl/

[4] Carmichael M. (2010). "Panair" Retrieved 15.3., 2012, from www.pdas.com

[5] Scholz, D. (2007). "A Student Project of a Blended Wing Body Aircraft: From Conceptual Design to Flight Testing." Presentation for EWADE 2007.

[6] Siegmann, H. (2008). "Aerodesign (in German)." Retrieved 15.3., 2012, from www.aerodesign.de.

[7] University of Illinois. "UIUC Airfoil Coordinates Database." Retrieved 15.3., 2012, from www.ae.illinois.edu/m-selig/ads/coord-database.html.

[8] Drela M. (2011). X-foil. Retrieved 15.3., 2012, from web.mit.edu/drela/Public/web/xfoil/

[9] Raymer D. (2005). Aircraft Design - A conceptual approach, AIAA

[10] Nelson, R. C. (1998). Flight Stability and Automatic Control, McGraw Hill.

[11] C.N.H. Lock, M. A. (1929). "Airscrew Body Interference: An Examination of a Method of Calculating the Mutual Effect of Airscrew and Body by the Strip Theory." Aircraft Engineering and Aerospace Technology, Vol. 1 Iss: 6, pp.207 - 209.

7.1 Copyright Statement